



UNIVERSITY OF LEEDS

This is a repository copy of *Unique Neoproterozoic carbon isotope excursions sustained by coupled evaporite dissolution and pyrite burial*.

White Rose Research Online URL for this paper:

<https://eprints.whiterose.ac.uk/149033/>

Version: Accepted Version

---

**Article:**

Shields, GA, Mills, BJW [orcid.org/0000-0002-9141-0931](https://orcid.org/0000-0002-9141-0931), Zhu, M et al. (3 more authors) (2019) Unique Neoproterozoic carbon isotope excursions sustained by coupled evaporite dissolution and pyrite burial. *Nature Geoscience*, 12 (10). pp. 823-827. ISSN 1752-0894

<https://doi.org/10.1038/s41561-019-0434-3>

---

© 2019, The Author(s), under exclusive licence to Springer Nature Limited. This is an author produced version of an article published in *Nature Geoscience*. Uploaded in accordance with the publisher's self-archiving policy.

**Reuse**

Items deposited in White Rose Research Online are protected by copyright, with all rights reserved unless indicated otherwise. They may be downloaded and/or printed for private study, or other acts as permitted by national copyright laws. The publisher or other rights holders may allow further reproduction and re-use of the full text version. This is indicated by the licence information on the White Rose Research Online record for the item.

**Takedown**

If you consider content in White Rose Research Online to be in breach of UK law, please notify us by emailing [eprints@whiterose.ac.uk](mailto:eprints@whiterose.ac.uk) including the URL of the record and the reason for the withdrawal request.



[eprints@whiterose.ac.uk](mailto:eprints@whiterose.ac.uk)  
<https://eprints.whiterose.ac.uk/>

1 Unique Neoproterozoic carbon isotope excursions sustained  
2 by coupled evaporite dissolution and pyrite burial

3

4 Graham A. Shields<sup>1</sup>, Benjamin J.W. Mills<sup>2</sup>, Maoyan Zhu<sup>3,4</sup>, Timothy D. Raub<sup>5</sup> Stuart  
5 Daines<sup>6</sup> & Timothy M. Lenton<sup>6</sup>

6

7 *<sup>1</sup>Department of Earth Sciences, University College London, Gower Place, London, WC1E*  
8 *6BT, UK*

9 *<sup>2</sup>School of Earth and Environment, University of Leeds, Leeds, LS2 9JT, UK*

10 *<sup>3</sup>State Key Laboratory of Palaeobiology and Stratigraphy & Center for Excellence in Life*  
11 *and Palaeoenvironment, Nanjing Institute of Geology and Palaeontology, Chinese Academy of*  
12 *Sciences, Nanjing, 210008, China*

13 *<sup>4</sup>College of Earth Sciences, University of Chinese Academy of Sciences, Beijing, 100049,*  
14 *China*

15 *<sup>5</sup>School of Earth and Environmental Sciences, University of St. Andrews, KY16 9AL, UK*

16 *<sup>6</sup>Global Systems Institute, University of Exeter, Exeter, EX4 4QE, UK*

17

18 Correspondence and requests for materials should be addressed to G.S.

19 ([g.shields@ucl.ac.uk](mailto:g.shields@ucl.ac.uk)), B.M ([b.mills@leeds.ac.uk](mailto:b.mills@leeds.ac.uk)) or M.Z. ([myzhu@nigpas.ac.cn](mailto:myzhu@nigpas.ac.cn))

20

21

22

23 **The Neoproterozoic Era witnessed a succession of biological innovations that culminated**  
24 **in a wide range of animal body plans and behaviours during the Ediacaran-Cambrian**  
25 **radiations. Intriguingly, this interval is also marked by perturbations to the global carbon**  
26 **cycle, as evidenced by extreme fluctuations in climate and carbon isotopes. The**  
27 **Neoproterozoic isotope record has defied parsimonious explanation because sustained**  
28  **$^{12}\text{C}$ -enrichment (low  $\delta^{13}\text{C}$ ) in seawater seems to imply that substantially more oxygen was**  
29 **consumed by organic carbon oxidation than could possibly have been available. Here we**  
30 **propose a solution to this problem, in which carbon and oxygen cycles can maintain**  
31 **dynamic equilibrium during negative  $\delta^{13}\text{C}$  excursions when surplus oxidant is generated**  
32 **through bacterial reduction of sulfate that originates from evaporite weathering.**  
33 **Coupling of evaporite dissolution with pyrite burial drives a positive feedback loop**  
34 **whereby net oxidation of marine organic carbon can sustain greenhouse forcing of**  
35 **chemical weathering, nutrient input and ocean margin euxinia. Our proposed model is**  
36 **particularly applicable to the late Ediacaran ‘Shuram’ isotope excursion that directly**  
37 **preceded the emergence of energetic metazoan metabolisms during the Ediacaran-**  
38 **Cambrian transition. Non-steady state sulfate dynamics are likely to have contributed to**  
39 **climate change, episodic ocean oxygenation and opportunistic radiations of aerobic life**  
40 **forms during the Neoproterozoic Era.**

41

42 The Neoproterozoic Era (1000 – c.540 Ma) marks a turning point in Earth history when groups  
43 of morphologically complex multicellular eukaryotes, including algae and animals, attained  
44 ecological dominance, irrevocably changing Earth System dynamics<sup>1</sup>. These biological  
45 radiations took place amid fluctuating climate, including two prolonged episodes of global  
46 glaciation during the Cryogenian Period (c.715 – c.660 and c.650 – c.635 Ma) and short-lived,  
47 regional ice ages during the Ediacaran Period (e.g. c.580 Ma), interspersed with warmer

48 intervals. The world's oceans also became episodically more oxygenated during the  
49 Neoproterozoic with the extent of oxygenated seafloor reaching near-modern levels at times  
50 during the early Cambrian<sup>2</sup>. Both climate and oxygenation are regulated by Earth's long-term  
51 carbon cycle, and so perhaps unsurprisingly this interval is characterised by extreme carbon  
52 isotope instability<sup>3</sup> (Fig. 1). Since their discovery over 30 years ago<sup>4-7</sup>, the uniquely high  
53 amplitudes of Neoproterozoic  $\delta^{13}\text{C}$  excursions have defied conventional interpretation<sup>3,8-10</sup>.  
54 Here we relate the largest of these anomalies to the transfer of oxidant from the evaporite rock  
55 reservoir to the surface environment via the coupling of sulfate weathering and pyrite burial.  
56 Such pulses of evaporite weathering are predicted to have occurred during the Ediacaran Period  
57 (see detailed account in SI 4), in particular, as Rodinia's passive margins underwent tectonic  
58 uplift during the amalgamation of Gondwanaland<sup>11</sup>.

59 Conventional carbon isotope mass balance is based on the principle that the isotopic  
60 composition of carbon input via outgassing and weathering, and that of sedimentary carbon  
61 outputs are equal on time scales of  $>10^5$  years. This  $\delta^{13}\text{C}$  value is considered to be unchanging  
62 at -5‰, which is taken to be the average composition of crustal carbon. Because organic matter  
63 is depleted in  $^{13}\text{C}$ , and carbonate rocks precipitate in isotopic equilibrium with ambient  
64 dissolved inorganic carbon (DIC), the mean  $\delta^{13}\text{C}$  value of carbonate rocks and fossils can be  
65 used to determine the proportion that sedimentary organic matter makes up of the total  
66 sedimentary carbon sink. This proportion is generally referred to as  $f_{\text{org}}$ , which has varied over  
67 Earth history between 0.1 and 0.3<sup>12</sup>. During the Neoproterozoic Era, globally correlative  
68 marine carbonate rocks from at least three intervals (~720 Ma Garvellach<sup>13</sup>, ~650 Ma  
69 Trezona<sup>14,15</sup>, ~560 Ma Shuram<sup>5,16</sup>/Wonoka<sup>7</sup>/DOUNCE<sup>17</sup> anomalies) are characterised by  $\delta^{13}\text{C}$   
70 values below -5‰ (Fig. 1), which can, using a conventional mass balance approach, only be  
71 explained by negative rates of organic burial. This is particularly true of the late Ediacaran  
72 Shuram excursion, during which  $\delta^{13}\text{C}$  remained below -8‰ for at least ~10 Myr<sup>18,19</sup>. In order

73 to address this quandary, it was proposed that the pool of dissolved organic matter (DOM) in  
74 the Proterozoic ocean was much larger than today, and that negative excursions represent non-  
75 steady-state remineralisation of that pool<sup>3</sup>. However, later numerical treatments of this  
76 model<sup>20,21</sup> pointed out that the Earth system cannot remain out of oxygen (and carbon) balance  
77 for such a long period of time. In other words, there is insufficient oxidant even in the modern  
78 atmosphere and oceans to remineralise enough organic matter to drive a -8‰  $\delta^{13}\text{C}$  excursion  
79 for several million years. As a result, many authors have interpreted extreme negative  
80 anomalies as diagenetic alteration<sup>22</sup>, authigenic cements<sup>10</sup> or as regional phenomena<sup>23</sup>.  
81 However, such arguments appeal to an inexplicable sampling bias, whereby globally  
82 correlative isotopic signatures are presumed to be unrepresentative of the global carbonate sink.  
83 Here we take a different approach to the problem of negative  $\delta^{13}\text{C}$  excursions by viewing them  
84 in terms of a linked carbon-sulfur-oxygen system, whereby changes in oxidant dynamics  
85 caused an excess of organic carbon oxidation over burial, resulting in a smaller DOM reservoir.  
86 For steady state to be maintained throughout a negative  $\delta^{13}\text{C}$  excursion, shrinkage of the DOM  
87 pool would need to match surplus oxidant production for the duration of the anomaly. If we  
88 consider plausible  $\delta^{13}\text{C}$  values of -10‰<sup>17</sup> and -35‰ for deposited carbonates and kerogen  
89 (globally averaged carbon sinks), respectively, and -30‰<sup>24</sup> and -5‰ for the DOM reservoir  
90 and crustal carbon (globally averaged carbon sources), respectively, then organic carbon  
91 oxidation would need to increase over the background rate by approximately a factor of three  
92 (Methods 1). This oxidant imbalance then requires three times as much oxygen as could have  
93 been supplied by organic burial alone. Therefore, it can only plausibly be sustained via the  
94 other major net source of oxygen to the Earth system: pyrite burial.

95 Although bacterial sulfate reduction coupled with pyrite burial releases on a mole-for-mole  
96 basis almost twice as much oxygen as organic burial<sup>25</sup>, it is generally assumed that the oxygen  
97 released by pyrite burial is approximately matched by the oxygen consumed during pyrite

98 weathering. However, most riverine sulfate derives from the weathering of evaporites<sup>26</sup>, rates  
99 of which due to the sporadic and regional nature of evaporite deposits, will vary considerably  
100 over time<sup>27</sup>. During parts of the Proterozoic, when oceans were both iron-rich and anoxic<sup>28</sup>,  
101 and so prone to sulfate reducing conditions (euxinia) at productive margins, one might  
102 realistically suppose that the amount of oxidising power transferred from rock sulfate to the  
103 surface environment would also have varied considerably, particularly during times when no  
104 basin-scale evaporite deposits were forming.

105 By writing a simple steady state mass-balance for the surface carbon cycle (Methods 1) we can  
106 map the broad relationship between the evaporite sulfate input rate, net DOM oxidation and  
107  $\delta^{13}\text{C}$  composition of the ocean-atmosphere system (Fig. 2). These calculations show that an  
108 evaporite weathering flux of around  $1.1 \times 10^{13}$  mol S yr<sup>-1</sup> (around 10 times the modern flux,  
109 as proposed for the dissolution event during the early Cenozoic<sup>27</sup>) could sustain a carbon  
110 isotope excursion of between -10‰ and -15‰, depending on the proportion of the riverine  
111 sulfate flux that is eventually buried as pyrite. Thus, the amount of oxidant required to achieve  
112 a deep negative carbon isotope excursion through net organic carbon oxidation may reasonably  
113 result from basin-scale evaporite dissolution.

114 Although plausible, we acknowledge that the above steady-state approximation is highly  
115 idealised and does not capture the true dynamics of the expected events, which include both  
116 positive and negative feedbacks (Fig. 3). For a negative  $\delta^{13}\text{C}$  excursion to be generated, oxidant  
117 input needs to be coupled to shrinkage of a marine DOM reservoir, rather than accumulating  
118 as an atmospheric oxygen increase. The rate of DOM oxidation is controlled by the deep ocean  
119 redox state, which itself is largely controlled by the abundance of atmospheric oxygen.  
120 Therefore, the process of DOM oxidation must be self-limiting and it should not be possible to  
121 deplete the surface oxygen reservoir beyond the level that causes the deep ocean to become  
122 entirely anoxic. Net oxidation of organic carbon should cause a substantial rise in atmospheric

123 CO<sub>2</sub> concentration and hence additional climate feedbacks. Rising CO<sub>2</sub> and temperature would  
124 support enhanced continental weathering, with the potential to drive further evaporite  
125 dissolution and therefore sustain oxidant delivery.

126 The network of long-term biogeochemical feedbacks between the sulfur, carbon and oxygen  
127 cycles is adequately represented by the COPSE biogeochemical box model<sup>29</sup>, and in order to  
128 explore how changes in the evaporite sulfate weathering flux might affect the oxidant balance  
129 in a Proterozoic marine environment, we modify COPSE to include a dynamic reservoir of  
130 deep-ocean DOM (modelled as DOC) and an extra input flux of sulfate from weathering  
131 (Methods 2 and SI). The model is first set up for an ‘Ediacaran like’ steady state ( $pO_2 = 0.05$   
132 PAL,  $pCO_2 = 13$  PAL,  $SO_4 = 0.1$  of present ocean level and a mostly anoxic deep ocean). This  
133 is achieved by fixing background tectonic parameters (uplift, degassing) at assumed values for  
134 600 Ma, while lowering the phosphorus input rate by 50%<sup>30</sup>.

135 We then perturb the system by adding a weathering pulse of sulfate from evaporite dissolution,  
136 and a smaller pulse of sulfate from pyrite oxidation, assuming that pyrite-bearing sediments  
137 would also be exposed during uplift. These pulses follow simple stepwise increases and  
138 decreases<sup>27</sup>, but also include a dependence on climate through runoff as summarized in figure  
139 3 (see methods for details). Figure 4a shows the overall amount of S delivery from evaporite  
140 dissolution ( $\sim 50 - \sim 100 \times 10^{18}$  mol), which is chosen to be similar to that proposed for  
141 basin-scale evaporite dissolution in the Cenozoic ( $\sim 1.1 \times 10^{13}$  mol S yr<sup>-1</sup> for  $\sim 5$  Myrs)<sup>27</sup>,  
142 although we use a longer timeframe to compare to the long duration of the Shuram excursion.  
143 The control model run with no DOC reservoir is shown in grey in figure 4. As shown  
144 previously<sup>27</sup>, this level of sulfate input raises ocean sulfate concentration considerably.  
145 Increased burial of pyrite leads to a substantial increase in  $pO_2$  and less prevalence of anoxia  
146 (shown as fraction of anoxic seafloor). Oxidative weathering of fossil organic carbon increases  
147 as O<sub>2</sub> rises, causing a small reduction in  $\delta^{13}C$  and increase in  $pCO_2$ . Seawater  $\delta^{34}S$  decreases

148 during the evaporite dissolution event as the combined  $\delta^{34}\text{S}$  value of inputted evaporite and  
149 pyrite sulfur is lower than the initial seawater value (we set  $\delta^{34}\text{S}_{\text{pyr}} = 0\text{‰}$  and  $\delta^{34}\text{S}_{\text{evap}} = 15\text{‰}$   
150 for the weathered material cf.<sup>31</sup>). The increase in pyrite burial buffers against this change by  
151 driving  $\delta^{34}\text{S}$  to more positive values (manifest as a ‘hump’ in the model  $\delta^{34}\text{S}$  curve), but is  
152 insufficient to reverse the overall trend.

153 We view net oxidation of deep ocean DOC as a feedback process driven by other model  
154 variables, and model it accordingly. Model runs include a DOC reservoir of size 20 times (light  
155 blue) and 30 times (dark blue) the modern DIC reservoir, respectively. The reservoir is assumed  
156 to have a carbon isotopic composition of  $-30\text{‰}$  and is allowed to be oxidized when the degree  
157 of anoxia (*ANOX*) is reduced below a threshold value (see Methods 2). In both runs, oxidation  
158 of DOC begins as the deep ocean becomes more widely oxygenated, however, as DOC  
159 oxidation is an oxygen sink, *ANOX* remains at the threshold value until the DOC reservoir  
160 nears depletion. In this period, the model is in a quasi-steady state wherein the transition to an  
161 oxygenated deep ocean is prevented by the net oxidation of DOC. During this state, ocean  $\delta^{13}\text{C}$   
162 is around  $-9\text{‰}$ , close to the value suggested by the simple calculations shown in Figure 2 for  
163 this level of sulfate input. Persistent anoxia, nutrient delivery, and the related increase in pyrite  
164 burial rates drive  $\delta^{34}\text{S}$  values higher than the control run, but the model still produces a negative  
165 excursion in  $\delta^{34}\text{S}$ , consistent with available observations<sup>16,32</sup>. On depletion of the DOC  
166 reservoir, the deep ocean can be oxygenated, and the model gradually returns to follow the  
167 control experiment.

168 The duration of the carbon isotope anomaly in our COPSE model reconstruction depends on  
169 the size of the DOM pool and on being able to maintain high rates of pyrite burial, but crucially  
170 does not depend on (or deplete) the atmospheric  $\text{O}_2$  pool, which is predicted to increase during  
171 the course of the excursion. A high rate of pyrite burial would be maintained in part due to the  
172 effect of organic remineralisation on raising  $p\text{CO}_2$  and global temperatures, which produces a



173 positive feedback loop (Fig. 3), whereby high chemical weathering rates and nutrient input can  
174 sustain euxinic ocean margins until either the DOM pool or the evaporite weathering flux  
175 decreases below a certain threshold value. Our treatment of these aspects is necessarily simple:  
176 we assume in the model run shown that 80% of the inputted sulfate is buried as pyrite by a  
177 near-shore biota that is sensitive to river inputs<sup>33</sup>. We also assume that gypsum, pyrite and  
178 organic carbon weathering fluxes are related to the model global rate of runoff (in addition to  
179 following a prescribed stepwise increase and decrease for pyrite and gypsum). We show further  
180 model runs in the SI in which the climate-weathering effect is not considered, and in which  
181 only evaporite inputs are considered, without any weathering of pyrite. We also show runs  
182 where differing amounts of P release from DOM oxidation fuels additional primary  
183 productivity. Sustained, highly-negative  $\delta^{13}\text{C}$  excursions remain possible in all of these cases,  
184 but a closely corresponding negative  $\delta^{34}\text{S}$  excursion can only be achieved when a smaller pulse  
185 of pyrite weathering accompanies the evaporite weathering pulse. While pyrite weathering is  
186 important in setting seawater  $\delta^{34}\text{S}$  values, pyrite weathering and deposition form an  $\text{O}_2$ -neutral  
187 cycle over long timescales so other model processes are relatively unaffected.

188 This evaporite dissolution / DOM oxidation scenario appears to be the most parsimonious  
189 solution to the Shuram C-isotope conundrum in that it predicts the extent of oxic seafloor to  
190 increase towards the end of the excursion, while maintaining high sulfate concentrations, which  
191 is in line with geochemical studies<sup>34,35</sup>. Furthermore, the Shuram anomaly coincided with  
192 orogenic uplift relating to the formation of Gondwanaland<sup>36</sup>, and in particular the tectonic  
193 inversion of all major basin-scale evaporite sulfate deposits of Tonian age (see SI 4). Although  
194 our model fits best the late Ediacaran Shuram anomaly, coupled evaporite dissolution and  
195 pyrite burial may have also played a role in other extreme negative carbon isotope excursions  
196 of the Neoproterozoic, which all occurred after one of the largest evaporite depositional events  
197 in Earth history between c.830 Ma and c.770 Ma<sup>37</sup>. The succeeding interval of major carbon

198 cycle disruption from c.770 Ma until c.550 Ma was a time of little or no basin-scale evaporite  
199 deposition, suggesting that, as in the Cenozoic<sup>5</sup>, the sulfate weathering-deposition cycle was  
200 not in steady-state. However, unlike the Cenozoic, the low atmospheric oxygen and anoxic  
201 deep ocean of the Neoproterozoic allowed evaporite-derived oxidizing power to be effectively  
202 transmitted into a negative  $\delta^{13}\text{C}$  signal.

203 The existence of a series of negative carbon isotope excursions during much of the  
204 Neoproterozoic Era indicates that the DOM pool underwent dynamic size changes throughout  
205 this time, and served as a buffer against oxygenation and climate change, but only when the  
206 pool was sufficiently large. Exhaustion of the DOM pool may have occurred during the Shuram  
207 anomaly, suggesting that the expansion of aerobic Ediacaran fauna at that time was an  
208 opportunistic radiation in response to a transient oxidant surplus. But it is possible that a  
209 greatly-reduced DOM pool may have continued to wax and wane until well into the Cambrian  
210 Period, during which time geochemical evidence suggests that redox conditions on the seafloor  
211 reached modern proportions for the first time<sup>2</sup>.

212

## 213 **Acknowledgements**

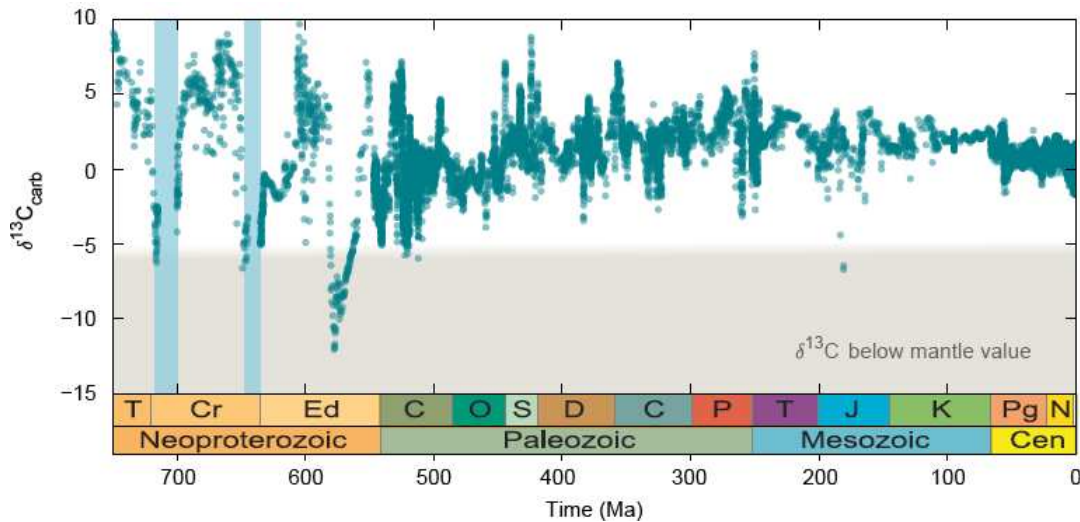
214 This work was supported by the NERC-NSFC programme 'Biosphere Evolution, Transitions and  
215 Resilience' through grant NE/P013643/1 to G.A.S. and M.Z. and NE/P013651/1 to T.M.L., by  
216 grant NE/R010129/1 to G.A.S. and B.J.W.M., a University of Leeds Academic Fellowship to  
217 B.J.W.M., and by the National Natural Science Foundation of China (41661134048) and  
218 Strategic Priority Research Program (B) of the Chinese Academy of Sciences (XDB18000000)  
219 to M.Z.

## 220 **Author contributions**

221 G.A.S. and B.J.W.M. conceived the project. B.J.W.M. created the model, which was revised  
222 from previous versions created by T.M.L., B.J.W.M. and S.D. All authors contributed to data  
223 interpretation and the writing of the manuscript.

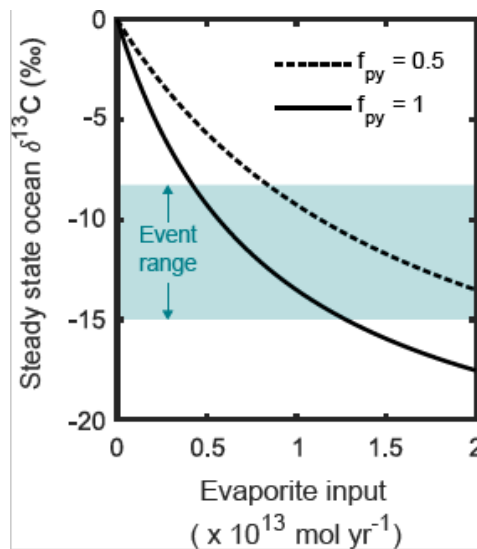
224

225



226

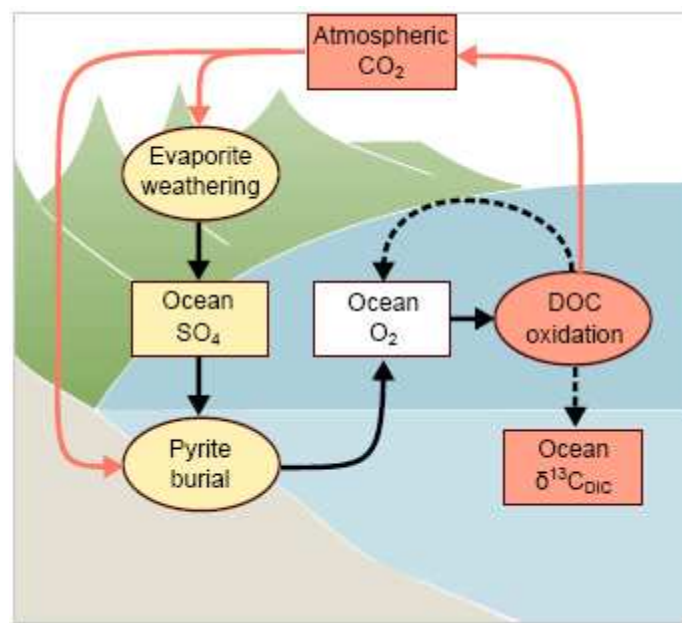
227 **Figure 1. Carbonate carbon isotope record (reproduced from <sup>38</sup>).** Grey area indicates values  
 228 below the average continental crust and mantle value of between -5‰ and -6‰ with three  
 229 major excursions at ~720 (Garvella anomaly<sup>13</sup>), ~650 (Trezona anomaly<sup>14</sup>) and ~560 Ma  
 230 (Shuram anomaly<sup>5,16</sup>). Smaller post-glacial excursions occur after Cryogenian (Sturtian and  
 231 Marinoan) low latitude glacial events (blue bars). Black dashed line indicates progressive  
 232 deep ocean oxygenation between ~580 and ~520 Ma<sup>39-41</sup>. Note that excursions to below the  
 233 mantle value occur before and during deep-ocean oxygenation and climate events.



234

235 **Figure 2. Negative carbon isotope excursion driven by net oxidation of a dissolved organic**  
 236 **carbon reservoir via coupled evaporite weathering and pyrite burial.** The magnitude of the

237  $\delta^{13}\text{C}$  anomaly depends on the  $\text{O}_2$  production rate from pyrite burial, which results from the  
238 evaporite weathering flux and the fraction of this flux that is buried as pyrite.

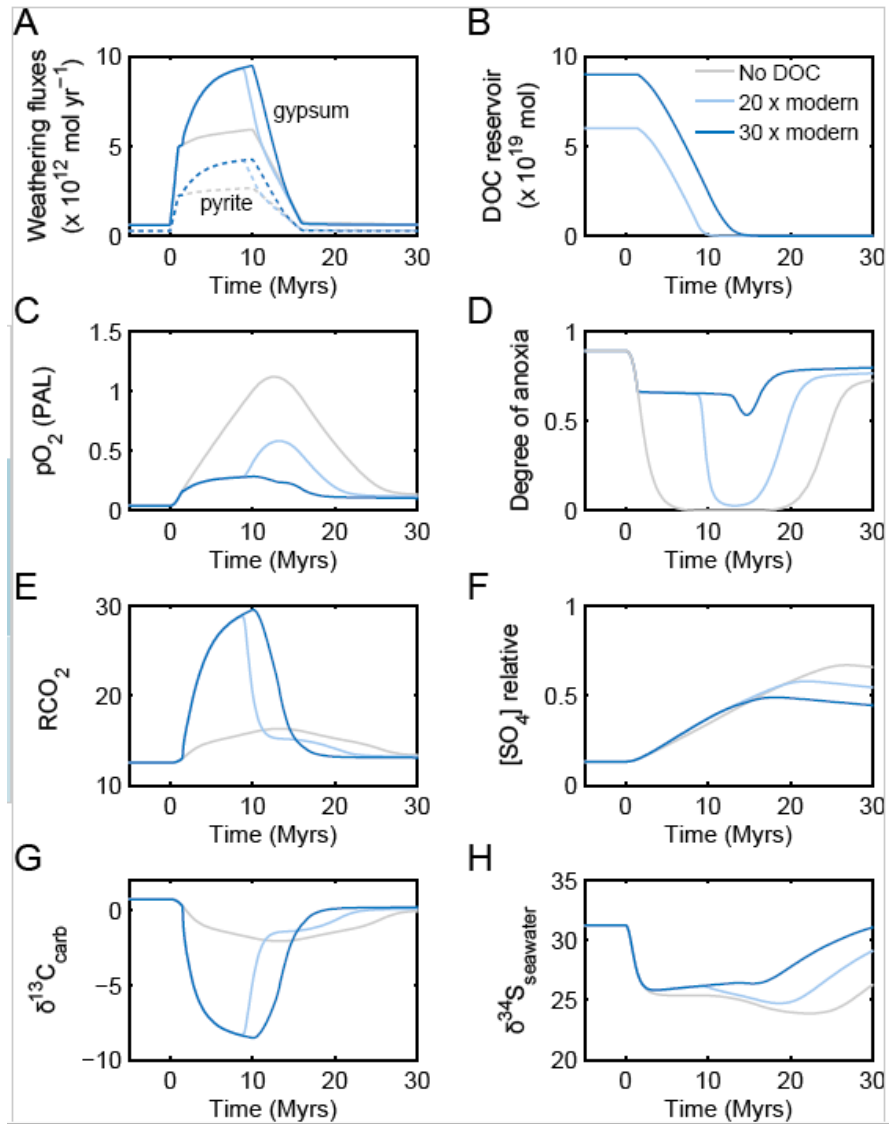


239

240 **Figure 3. Feedback diagram illustrating the effects of evaporite weathering on ocean**  
241 **oxygenation and  $\delta^{13}\text{C}$ .** Boxes show quantities, ovals show processes, whilst yellow indicates  
242 sulfur cycle and red indicates carbon cycle. An evaporite dissolution event results in a large  
243 flux of sulfate to the ocean, permitting high rates of pyrite burial, which increases  
244 atmospheric and ocean  $\text{O}_2$ . As the deep ocean becomes oxygenated, depletion of the dissolved  
245 organic carbon (DOC) reservoir represents a negative feedback on ocean oxygenation and  
246 drives ocean  $\delta^{13}\text{C}$  to negative values. Red arrows show potential for positive feedback: DOC  
247 oxidation increases atmospheric  $\text{CO}_2$ , leading to higher surface temperature and greater  
248 rates of precipitation and runoff, which fuels further evaporite dissolution and nutrient  
249 delivery. Solid arrows show positive effects and dashed arrows show negative effects.

250

251



252  
253

254 **Figure 4. COPSE Model forced with sulfate input and including differently sized DOC**  
 255 **reservoirs.** A. Input rates of sulfate from gypsum and pyrite weathering. B. Size of DOC  
 256 reservoir in moles of carbon. C. A. Relative atmospheric oxygen concentration. D. Degree of  
 257 ocean anoxia. E. Relative atmospheric carbon dioxide concentration. F. Relative ocean sulfate  
 258 concentration. G. Calculated  $\delta^{13}\text{C}$  of new carbonate. H. Calculated seawater  $\delta^{34}\text{S}$ .

259  
260

## 261 **Methods**

### 262 **1. Steady state mass balance calculations**

263 In order to estimate the surplus oxygen flux needed to sustain the late Ediacaran Shuram  
264 anomaly, we apply standard isotope mass balance, and assume  $\delta^{13}\text{C}$  values of  $-10\text{‰}^{17}$  and -  
265  $35\text{‰}$  for deposited carbonates ( $\delta^{13}\text{C}_{\text{carb}}$ ) and kerogen ( $\delta^{13}\text{C}_{\text{org}}$ ), respectively, and  $-30\text{‰}^{24}$  and -  
266  $5\text{‰}$  for the integrated carbon sources ( $\delta^{13}\text{C}_{\text{input}}$ ) of DOM oxidation and crustal carbon,  
267 respectively. Following standard C-isotope mass balance,  $\delta^{13}\text{C}_{\text{carb}} = (\Delta^{13}\text{C}_{\text{carb-org}}) \cdot f_{\text{org}} +$   
268  $\delta^{13}\text{C}_{\text{input}}$  at steady state, and so during the excursion when  $f_{\text{org}} = 0.1^{12}$ , then  $\delta^{13}\text{C}_{\text{input}} = -12.5\text{‰}$ .  
269 The proportion that DOM oxidation contributed to the global carbon cycle, i.e.  $f_{\text{DOM}} = 0.3$ ,  
270 whereby  $\delta^{13}\text{C}_{\text{excursion input}} = -12.5\text{‰} = \delta^{13}\text{C}_{\text{pre-excursion input}} (1-f_{\text{DOM}}) + \delta^{13}\text{C}_{\text{DOM}} \cdot f_{\text{DOM}}$ . A  
271 conservative estimate for the requisite surplus oxygen flux ( $f_{\text{DOM}}$ ) would therefore be about  
272 three times greater than that supplied by organic burial ( $f_{\text{org}}$ ) alone, thus requiring a  
273 contribution from other sources, most likely pyrite burial.

274 In order to explore the potential for evaporite dissolution to drive surface system  
275 oxygenation and negative carbon isotope excursions, we first solve a simple isotope mass  
276 balance calculation for the  $\delta^{13}\text{C}$  composition of the total combined atmosphere and ocean  
277 carbon pool (A). Variations in A over time follow the formulation:

$$278 \quad \frac{dA}{dt} = F_{\text{oxidw}} + F_{\text{ocdeg}} + F_{\text{carbw}} + F_{\text{ccdeg}} - F_{\text{ocb}} - F_{\text{mccb}} - F_{\text{sffw}} + F_{\text{DOCox}} \quad (1)$$

279 Where  $F_{\text{oxidw}}$  is oxidative weathering,  $F_{\text{ocdeg}}$  is organic carbon metamorphism and  
280 degassing,  $F_{\text{carbw}}$  is carbonate weathering,  $F_{\text{ccdeg}}$  is carbonate degassing,  $F_{\text{ocb}}$  is organic  
281 carbon burial,  $F_{\text{mccb}}$  is marine carbonate burial and  $F_{\text{sffw}}$  is seafloor weathering  
282 (following<sup>29,21</sup>). We add  $F_{\text{DOCox}}$  to represent the oxidation of a deep ocean reservoir of  
283 dissolved organic carbon. As a general approximation to the expected Ediacaran carbon cycle  
284 we take  $F_{\text{oxidw}} = 2.5 \times 10^{12} \text{ mol yr}^{-1}$ ,  $F_{\text{ocdeg}} = 0.5 \times 10^{12} \text{ mol yr}^{-1}$ ,  $F_{\text{carbw}} = 8 \times 10^{12} \text{ mol}$

285  $\text{yr}^{-1}$ ,  $F_{ccdeg} = 6 \times 10^{12} \text{ mol yr}^{-1}$ ,  $F_{ocb} = 3 \times 10^{12} \text{ mol yr}^{-1}$ ,  $F_{mccb} = 12 \times 10^{12} \text{ mol yr}^{-1}$ , and  
 286  $F_{sfw} = 2 \times 10^{12} \text{ mol yr}^{-1}$ . Here  $\frac{dA}{dt} = 0$ , thus the carbon cycle is in steady state, and the  
 287 fraction of carbon buried in organic form ( $f_{org}$ ) is 0.2.

288 We assume that the sulfur cycle begins at steady state, and allow an addition of sulfate  
 289 from evaporite dissolution,  $F_{evap}$  (in moles S). To maintain long-term steady state this  
 290 evaporite must leave the system in oxidised (e.g. gypsum) or reduced (e.g. pyrite) forms. We  
 291 denote  $f_{py}$  as the fraction of the evaporite input that exits the system as pyrite and experiment  
 292 with values of 0.5 and 1. Assuming that DOC oxidation is driven solely by excess oxygen  
 293 produced by burial of pyrite, we set the flux of DOC oxidation as  $F_{DOCox} = 2 \times f_{py} F_{evap}$ . To  
 294 maintain long term steady state in the carbon cycle, the flux of additional  $\text{CO}_2$  from DOC  
 295 oxidation must be balanced by burial of carbonates and organic carbon. We assume this  
 296 occurs at the initial ratio of 4:1 in favour of carbonates (e.g.  $f_{org} = 0.2$ ). Thus the equation  
 297 for long term carbon isotopic mass balance is:

$$298 \quad F_{oxidw} \delta_G + F_{ocdeg} \delta_G + F_{carbw} \delta_C + F_{ccdeg} \delta_C - F_{ocb} (\delta_A - \Delta B) - F_{mccb} \delta_A - F_{sfw} \delta_A +$$

$$299 \quad F_{DOCox} \delta_{DOC} - 0.2 F_{DOCox} (\delta_A - \Delta B) - 0.8 F_{DOCox} \delta_A = 0 \quad (2)$$

300 where  $\delta_A$  is the isotopic composition of atmosphere and ocean carbon,  $\delta_C$  is the compositions  
 301 of buried carbonates,  $\delta_G$  is the composition of buried organic carbon and  $\delta_{DOC}$  is the  
 302 composition of the oceanic DOC reservoir. We take  $\delta_C = 0\%$ ,  $\delta_G = -25\%$ ,  $\Delta B = 25\%$ ,  
 303  $\delta_{DOC} = -30\%$ , and solve for  $\delta_A$  under varying values for  $F_{evap}$ . Results are shown in figure  
 304 2.

305

## 306 2. COPSE model reconstructions

307 We run the COPSE model<sup>21</sup> to steady state under assumed Ediacaran forcings, add a  
308 deep ocean reservoir of dissolved organic carbon that responds to the degree of ocean anoxia,  
309 then impose an evaporite dissolution and pyrite burial event.

### 310 *Ediacaran steady state*

311 The ‘Ediacaran’ steady state is achieved by fixing all model parameters at the assumed  
312 values for 600 Ma. In all but two cases, these values are assumed to be the same as at the  
313 beginning of the Phanerozoic, but we lower the rate of phosphorus input by 50% to reduce  
314 atmospheric oxygen (e.g. as in Daines et al. 2017<sup>22</sup>) and use a static gypsum burial rate of  
315 50% of the present day to reduce ocean sulfate. The steady state has  $pO_2 = \sim 0.05$  PAL,  $pCO_2$   
316  $= \sim 13$  PAL,  $SO_4 = \sim 0.1$  of present ocean level and a mostly anoxic deep ocean ( $ANOX \approx 0.9$ ).

### 317 *Dissolved organic carbon reservoir*

318 The size of the model DOC reservoir is set at the beginning of the model run. The  
319 reservoir has a single output flux via DOC oxidation, which depends on the degree of ocean  
320 anoxia ( $ANOX$ ):

$$321 \quad \frac{dDOC}{dt} = \begin{cases} 0, & DOC < 1 \times 10^{12} \text{ mol} \\ -\frac{k}{1+e^{-a(1-ANOX-c)}} \left(\frac{DOC}{DOC_0}\right), & DOC \geq 1 \times 10^{12} \text{ mol} \end{cases} \quad (3)$$

322 here  $a = 300$ ,  $c = 0.35$  and  $k = 1 \times 10^{14} \text{ mol yr}^{-1}$  are scaling parameters for the sigmoid  
323 function, which define the anoxia level at which DOC oxidation begins and the rapidity of the  
324 transition. In practice, this function allows for geologically-rapid oxidation of DOC when  
325  $ANOX < 0.7$ . The threshold here is chosen to be slightly below the model steady state so that  
326 the DOC reservoir is stable under the COPSE Ediacaran setup. DOC oxidation is terminated  
327 when the reservoir becomes smaller than  $10^{12}$  moles, rather than zero, to prevent system  
328 instability. The rate of DOC oxidation is controlled by  $O_2$  supply and never reaches the value



329 of  $k$ . This is shown in the SI for different values of  $c$ . We assume that DOC is oxidised  
330 directly by  $O_2$ , although oxidation via microbial sulfate reduction is also possible.

### 331 ***Sulfate input***

332 An uplift and evaporite dissolution event is prescribed in the model using a simple  
333 step-forcing that follows previous work on evaporite dissolution<sup>5</sup>. The time-dependent  
334 forcing function for sulfate input is:

$$335 \quad S_{input} = [0 \ 1 \ 10 \ 16], [0 \ 7 \ 7 \ 0] \quad (4)$$

336 where the first bracket is time in million years and the second bracket is the additional sulfate  
337 input in terms of the background weathering fluxes. For the model run in the manuscript,  
338 steady state ‘background’ and additional ‘pulse’ inputs of both pyrite and gypsum are  
339 considered:

$$340 \quad gypw_{background} = k_{gypw} \cdot g_{runoff} \quad (5)$$

$$341 \quad gypw_{pulse} = k_{gypw} \cdot g_{runoff} \cdot S_{input} \quad (6)$$

$$342 \quad pyrw_{background} = k_{pyrw} \cdot g_{runoff} \quad (7)$$

$$343 \quad pyrw_{pulse} = k_{pyrw} \cdot g_{runoff} \cdot S_{input} \quad (8)$$

344 here  $k_{gyp}$  and  $k_{pyr}$  are the present day weathering rates of gypsum and pyrite, and  $g_{runoff}$  is a  
345 climate-dependence representing the effect of global runoff on weathering fluxes, e.g. Berner  
346 (1994)<sup>42</sup>:

$$347 \quad g_{runoff} = 1 + 0.087(T - T_0) \quad (9)$$

348 where  $T$  is global average surface temperature and  $T_0$  is the present day value.

### 349 ***Sulfate burial***

350 The COPSE model assumes that sulfate burial fluxes are linearly proportional to the  
351 total oceanic sulfate concentration, which means that concentration would have to rise to  
352 many times the present day level in order to bury large amounts of pyrite. We add an  
353 additional flux of pyrite burial ( $mpsb_{additional}$ ) that is directly related to the pulsed weathering  
354 input of sulfate, so pyrite burial is more clearly related to the sulfate supply to high-  
355 productivity near-shore environments. A partitioning constant  $f_{py}$  is used to determine what  
356 fraction of the pulsed sulfate input is buried as pyrite. This is set at 0.8 in the plot shown in  
357 the ms. Additional sulfate that is not buried as pyrite is assumed to be buried as gypsum:

$$358 \quad mpsb_{additional} = f_{py} \cdot (pyrw_{pulse} + gypw_{pulse}) \quad (10)$$

$$359 \quad mgsb_{additional} = (1 - f_{py}) \cdot (pyrw_{pulse} + gypw_{pulse}) \quad (11)$$

360

### 361 ***Other model alterations***

362 The following alterations are made to COPSE to make the model more applicable to  
363 the scenario being tested:

364

- 365 1. COPSE uses a sigmoid function to calculate the degree of ocean anoxia, *ANOX*. A  
366 modified version of the function was previously presented<sup>30</sup>, based on the anoxia  
367 response of 3D ocean models. Whilst the functions are similar and the choice  
368 makes little difference in the Phanerozoic version of COPSE, the Watson et al.  
369 version of the function has a more gradual transition to anoxia and allows the  
370 model to more easily assume an ‘Ediacaran-like’ steady state under minimal  
371 alteration of other parameters and is therefore used here.
- 372 2. COPSE predicts low  $\delta^{13}\text{C}$  values for the Ediacaran steady state ( $\sim -2\text{‰}$ ). In order  
373 to clearly test the size of the evaporite-induced excursion, we set the overall  
374 crustal carbonate reservoir  $\delta^{13}\text{C}$  value to  $2\text{‰}$ , which raises the  $\delta^{13}\text{C}$  value of

375 carbon inputs and makes newly formed  $\delta^{13}\text{C}_{\text{carb}}$  is  $\sim 0\%$ . This alteration merely  
376 shifts the baseline of  $\delta^{13}\text{C}$ .

377 3. We take crustal values of  $\delta^{34}\text{S}_{\text{pyrite}} = 0\%$  and  $\delta^{34}\text{S}_{\text{gypsum}} = 30\%$  to reproduce  
378 Ediacaran pre-excursion baseline values<sup>16</sup>, and assume that the pulse of evaporite  
379 weathering has  $\delta^{34}\text{S}_{\text{gypsum}} = 15\%$ .

380 4. COPSE has a relatively high rate of gypsum weathering and burial at present day,  
381 we alter the present day reference rate of gypsum weathering to  $1 \times 10^{12} \text{ mol S yr}^{-1}$ ,  
382 to better represent the background rate used in ref 5, for which our evaporite  
383 dissolution scenario is based.

### 384 **3. Additional model experiments**

385 See supplementary information 1 for additional model runs where we assume no  
386 climate dependence for sulfur weathering fluxes, and consider the role of pyrite versus  
387 gypsum weathering, and test uncertainty in the DOC oxidation function.

### 388 **4. Full model description**

389 See supplementary information 2 for full modified COPSE model equations and  
390 description. MATLAB code for COPSE is freely available at  
391 <https://github.com/sjdaines/COPSE/releases>

392

### 393 **References**

- 394 1. Lenton, T. M., Boyle, R. A., Poulton, S. W., Shields-Zhou, G. A. & Butterfield, N. J.  
395 Co-evolution of eukaryotes and ocean oxygenation in the Neoproterozoic era. *Nat.*  
396 *Geosci.* **7**, (2014).
- 397 2. Chen, X. *et al.* Rise to modern levels of ocean oxygenation coincided with the  
398 Cambrian radiation of animals. *Nat. Commun.* **6**, 1–7 (2015).

- 399 3. Rothman, D. H., Hayes, J. M. & Summons, R. E. Dynamics of the Neoproterozoic  
400 carbon cycle. *Proc. Natl. Acad. Sci. USA* **100**, 8124–8129 (2003).
- 401 4. Knoll, A. H., Hayes, J. M., Kaufman, a J., Swett, K. & Lambert, I. B. Secular  
402 variation in carbon isotope ratios from Upper Proterozoic successions of Svalbard and  
403 East Greenland. *Nature* **321**, 832–838 (1986).
- 404 5. Burns, S. J. & Matter, A. Carbon isotopic record of the latest Proterozoic from Oman.  
405 *Eclogae Geol. Helv.* **86**, 595–607 (1993).
- 406 6. Kaufman, A. J., Knoll, A. H. & Narbonne, G. M. Isotopes, ice ages, and terminal  
407 Proterozoic earth history. *Proc. Natl. Acad. Sci. U. S. A.* **94**, 6600–6605 (1997).
- 408 7. Calver, C. R. Isotope stratigraphy of the Ediacarian (Neoproterozoic III) of the  
409 Adelaide Rift Complex, Australia, and the overprint of water column stratification.  
410 *Precambrian Res.* **100**, 121–150 (2000).
- 411 8. Melezhik, V., Fallick, A. E. & Pokrovsky, B. G. Enigmatic nature of thick sedimentary  
412 carbonates depleted in <sup>13</sup>C beyond the canonical mantle value: The challenges to our  
413 understanding of the terrestrial carbon cycle. *Precambrian Res.* **137**, 131–165 (2005).
- 414 9. Grotzinger, J. P., Fike, D. a. & Fischer, W. W. Enigmatic origin of the largest-known  
415 carbon isotope excursion in Earth’s history. *Nat. Geosci.* **4**, 285–292 (2011).
- 416 10. Schrag, D. P., Higgins, J. A., Macdonald, F. A. & Johnston, D. T. Authigenic  
417 carbonate and the history of the global carbon cycle. *Science (80-. )*. **339**, 540–3  
418 (2013).
- 419 11. Li, Z. X. *et al.* Assembly, configuration, and break-up history of Rodinia: A synthesis.  
420 *Precambrian Res.* (2008). doi:10.1016/j.precamres.2007.04.021
- 421 12. Krissansen-Totton, J., Buick, R. & Catling, D. C. A statistical analysis of the carbon

- 422 isotope record from the Archean to Phanerozoic and implications for the rise of  
423 oxygen. *Am. J. Sci.* **315**, 275–316 (2015).
- 424 13. Fairchild, I. J. *et al.* Tonian-Cryogenian boundary sections of Argyll, Scotland.  
425 *Precambrian Res.* 1–28 (2017). doi:10.1016/j.precamres.2017.09.020
- 426 14. McKirdy, D. M. *et al.* A chemostratigraphic overview of the late Cryogenian  
427 interglacial sequence in the Adelaide Fold-Thrust Belt, South Australia. *Precambrian*  
428 *Research* **106**, 149–186 (2001).
- 429 15. Rose, C. V. *et al.* Constraints on the origin and relative timing of the Trezona ??  $^{13}\text{C}$   
430 anomaly below the end-Cryogenian glaciation. *Earth Planet. Sci. Lett.* **319–320**, 241–  
431 250 (2012).
- 432 16. Fike, D. A, Grotzinger, J. P., Pratt, L. M. & Summons, R. E. Oxidation of the  
433 Ediacaran ocean. *Nature* **444**, 744–7 (2006).
- 434 17. Lu, M. *et al.* The DOUNCE event at the top of the Ediacaran Doushantuo Formation,  
435 South China: Broad stratigraphic occurrence and non-diagenetic origin. *Precambrian*  
436 *Res.* **225**, (2013).
- 437 18. Condon, D. *et al.* U-Pb ages from the Neoproterozoic Doushantuo Formation, China.  
438 *Science* **308**, 95–98 (2005).
- 439 19. Gong, Z., Kodama, K. P. & Li, Y. X. Rock magnetic cyclostratigraphy of the  
440 Doushantuo Formation, South China and its implications for the duration of the  
441 Shuram carbon isotope excursion. *Precambrian Res.* **289**, 62–74 (2017).
- 442 20. Bristow, T. F. & Kennedy, M. J. Carbon isotope excursions and the oxidant budget of  
443 the Ediacaran atmosphere and ocean. *Geology* **36**, 863–866 (2008).
- 444 21. Bjerrum, C. J. & Canfield, D. E. Towards a quantitative understanding of the late

- 445 Neoproterozoic carbon cycle. *Proc. Natl. Acad. Sci. U. S. A.* **108**, 5542–5547 (2011).
- 446 22. Derry, L. A. A burial diagenesis origin for the Ediacaran Shuram-Wonoka carbon  
447 isotope anomaly. *Earth Planet. Sci. Lett.* **294**, 152–162 (2010).
- 448 23. Li, C. *et al.* Uncovering the spatial heterogeneity of Ediacaran carbon cycling.  
449 *Geobiology* **15**, 211–224 (2017).
- 450 24. Lee, C., Love, G. D., Fischer, W. W., Grotzinger, J. P. & Halverson, G. P. Marine  
451 organic matter cycling during the Ediacaran Shuram excursion. *Geology* **43**, 1103–  
452 1106 (2015).
- 453 25. Garrels, R. M. & Lerman, A. Coupling of the sedimentary sulfur and carbon cycles -  
454 an improved model. *Am. J. Sci.* 989–1007 (1984).
- 455 26. Burke, A. *et al.* Sulfur isotopes in rivers: Insights into global weathering budgets,  
456 pyrite oxidation, and the modern sulfur cycle. *Earth Planet. Sci. Lett.* (2018).  
457 doi:10.1016/j.epsl.2018.05.022
- 458 27. Wortmann, U. G. & Paytan, A. Rapid variability of seawater chemistry over the past  
459 130 million years. *Science (80-. ).* **337**, 334–336 (2012).
- 460 28. Guilbaud, R., Poulton, S. W., Butterfield, N. J., Zhu, M. & Shields-Zhou, G. A. A  
461 global transition to ferruginous conditions in the early Neoproterozoic oceans. *Nat.*  
462 *Geosci.* **8**, (2015).
- 463 29. Lenton, T. M., Daines, S. J. & Mills, B. J. W. COPSE reloaded: An improved model of  
464 biogeochemical cycling over Phanerozoic time. *Earth-Science Rev.* **178**, 1–28 (2017).
- 465 30. Daines, S. J., Mills, B. J. W. & Lenton, T. M. Atmospheric oxygen regulation at low  
466 Proterozoic levels by incomplete oxidative weathering of sedimentary organic carbon.  
467 *Nat. Commun.* **8**, (2017).

- 468 31. Canfield, D. E. & Farquhar, J. Animal evolution, bioturbation, and the sulfate  
469 concentration of the oceans. *Proc. Natl. Acad. Sci. U. S. A.* **106**, 8123–8127 (2009).
- 470 32. Osburn, M. R., Owens, J., Bergmann, K. D., Lyons, T. W. & Grotzinger, J. P.  
471 Dynamic changes in sulfate sulfur isotopes preceding the Ediacaran Shuram  
472 Excursion. *Geochim. Cosmochim. Acta* **170**, 204–224 (2015).
- 473 33. Laakso, T. A. & Schrag, D. P. A small marine biosphere in the Proterozoic.  
474 *Geobiology* (2019). doi:10.1111/gbi.12323
- 475 34. Kendall, B. *et al.* Uranium and molybdenum isotope evidence for an episode of  
476 widespread ocean oxygenation during the late ediacaran period. *Geochim. Cosmochim.*  
477 *Acta* **156**, 173–193 (2015).
- 478 35. Shi, W. *et al.* Sulfur isotope evidence for transient marine-shelf oxidation during the  
479 Ediacaran Shuram Excursion. *Geology* **46**, 267–270 (2018).
- 480 36. Campbell, I. H. & Squire, R. J. The mountains that triggered the Late Neoproterozoic  
481 increase in oxygen: The Second Great Oxidation Event. *Geochim. Cosmochim. Acta*  
482 **74**, 4187–4206 (2010).
- 483 37. Prince, J. K. G., Rainbird, R. H. & Wing, B. A. Evaporite deposition in the mid-  
484 Neoproterozoic as a driver for changes in seawater chemistry and the biogeochemical  
485 cycle of sulfur. *Geology* (2019). doi:10.1130/g45464.1
- 486 38. Saltzman, M. R. & Thomas, E. Chapter 11 - Carbon Isotope Stratigraphy. in *The*  
487 *Geologic Time Scale* 207–232 (2012). doi:http://dx.doi.org/10.1016/B978-0-444-  
488 59425-9.00011-1
- 489 39. Canfield, D. E., Poulton, S. W. & Narbonne, G. M. Late-Neoproterozoic Deep-Ocean  
490 Oxygenation and the Rise of Animal Life. *Science* (80-. ). **315**, 92–95 (2007).

- 491 40. Chen, X. *et al.* Rise to modern levels of ocean oxygenation coincided with the  
492 Cambrian radiation of animals. *Nat. Commun.* **6**, (2015).
- 493 41. Sahoo, S. K. *et al.* Oceanic oxygenation events in the anoxic Ediacaran ocean.  
494 *Geobiology* **14**, (2016).
- 495 42. Berner, R. A. GEOCARB II: a revised model of atmospheric CO<sub>2</sub> over Phanerozoic  
496 time. *Am. J. Sci.* (1994). doi:10.2475/ajs.294.1.56
- 497